Available online at www.sciencedirect.com
SCIENCE DIRECT
Journal of Catalysis 237 (2006) 368–380
JOURNAL OF CATALYSIS
www.elsevier.com/locate/jcat

Cu- and Pd-substituted nanoscale Fe-based perovskites for selective catalytic reduction of NO by propene

Runduo Zhang [a], Adrian Villanueva [a], Houshang Alamdari [b], Serge Kaliaguine [a,*]

[a] *Department of Chemical Engineering, Laval University, Ste Foy (Quebec), PQ G1K 7P4, Canada*
[b] *Nanox Inc., 4975 rue Rideau, Local 100, Ste Foy (Quebec), PQ G2E 5H5, Canada*

Received 12 August 2005; revised 8 November 2005; accepted 10 November 2005

Abstract

A series of Fe-based perovskites with high specific surface area was prepared by a new method, reactive grinding, and characterized by N_2 adsorption, XRD, SEM, H_2-TPR, TPD of O_2, TPD of $NO+O_2$, TPD of C_3H_6, and TPSR of $NO+O_2$ under C_3H_6/He flow. These materials were then subjected to activity tests in the selective catalytic reduction of NO by propene. The catalytic performance over $LaFeO_3$ is poor but can be improved significantly by incorporating Cu into its lattice, resulting in N_2 yields over $LaFe_{0.8}Cu_{0.2}O_3$ of 81% at 450 °C and 97% at 700 °C with a reactant mixture containing 3000 ppm NO, 3000 ppm C_3H_6, and 1% O_2 in helium at a space velocity of 50,000 h^{-1}. The enhanced NO reduction after Cu substitution is attributed to the easy formation of nitrate species, which have high reactivity toward C_3H_6. A mechanism was proposed with the formation of nitrate species as the first step and organo nitrogen compounds as important intermediates. Great catalytic performance at low temperature was also achieved over $LaFe_{0.97}Pd_{0.03}O_3$ with a N_2 yield of 67% and C_3H_6 conversion of 68% at 350 °C corresponding to the outstanding redox properties of this catalyst. O_2 can act as a promoter to oxidize NO into strongly adsorbed nitrate species, and also can accelerate the transformation of organo nitrogen compounds and isocyanate to get the desired products. In contrast, at higher concentrations O_2 has a detrimental effect, leading to consumption of the reducing agent by the complete oxidation of C_3H_6.
© 2006 Published by Elsevier Inc.

Keywords: SCR of NO; Propene; Reactive grinding; High surface area; Fe-based; Perovskite; TPR; TPD

1. Introduction

Perovskite oxides, promising alternatives to supported noble metals, have attracted much attention for exhaust gas depollution because of their low cost, thermal stability at rather high temperatures, great versatility, and excellent redox properties. Most previous studies on the use of perovskites for the purification of motor vehicles exhaust gas from NO_x have involved the reaction between NO and CO [1–3]. Much less work has been reported on NO reduction using propene as a reducing agent in the presence of oxygen over perovskite-type oxides. Moreover, the limited data related to $NO + C_3H_6 + O_2$ reaction over perovskites shows poor catalytic performance, with maximal NO conversion to N_2 of <25% [4,5]. Consequently, new efforts are needed to improve the catalytic activity toward NO reduction by C_3H_6 in the presence of O_2 over perovskites, aiming to satisfy the requirements for their practical application.

It is well known that the catalytic characteristics of perovskites for various reactions and their redox properties depend primarily on the preparation procedure. The conventional method of perovskite preparation, the so-called "ceramic method," involves a calcination step with a temperature of at least 800 °C. As a result, large grain size and low specific surface area are usually obtained with a value of several m^2/g or even less [6]. Some other methods for preparing perovskites, including microemulsion [7], spray-drying [8], freeze-drying [9], citrate complexation [10], co-precipitation [11], and the sol–gel process [12], were developed to increase the specific surface area of perovskites by means of synthesis and calcination at relatively low temperatures (500–600 °C). The specific surface areas of perovskites generated by the foregoing methods can reach 10–30 m^2/g. Recently, a new method for perovskite preparation—reactive grinding—has been proposed

* Corresponding author. Fax: +1 418 656 3810.
E-mail address: kaliagui@gch.ulaval.ca (S. Kaliaguine).

0021-9517/$ – see front matter © 2006 Published by Elsevier Inc.
doi:10.1016/j.jcat.2005.11.019

by our group, generating a wide variety of perovskites at room temperature with extraordinarily high specific surface areas (on the order of 100 m^2/g) when grinding additives are used [13–15].

The selection of B-site cations is of essential importance in designing perovskite catalysts as well as in modifying their catalytic properties, because the catalytic properties of perovskite-type oxides are practically determined by the nature of their B-site cations [16,17]. Fe-based perovskites were thought to be suitable catalysts for air pollution control because of their great performance in interactions between CO and NO [1], despite the scarcity of investigations into selective catalytic reduction of NO by C_3H_6 in the presence of O_2. Moreover, B-site substitution of perovskites was also considered an effective way to improve their catalytic properties due to the generation of new lattice defects, mixed valence states, and nonstoichiometric oxygen [18]. Copper-containing catalysts are of special interest because they are active in the transformation of nitrogen oxides [19], with the low-coordination isolated Cu ions as active sites [20,21]. In addition, the activity of Pd-substituted lanthanum cuprates was found to be comparable to that of Pt-Rh/CeO_2-Al_2O_3 for NO reduction and higher for CO and C_3H_6 oxidation [22]. A special self-regeneration character on Pd-containing perovskite was also described by Nishihata et al., who showed that Pd can move back and forth between the B-site in the perovskite and the metal oxide when exposed to fluctuations in the redox characteristics of the emission exhaust [23]. Cu and Pd ions, with valence states different from those of Fe ions in a perovskite lattice, thus may be interesting candidates for partial B-site substitution in $LaFeO_3$.

In the present study, a parent $LaFeO_3$ and its corresponding Cu- or Pd-substituted perovskites ($LaFe_{0.8}Cu_{0.2}O_3$ and $LaFe_{0.97}Pd_{0.03}O_3$), synthesized by reactive grinding, were characterized by X-ray diffraction (XRD), temperature-programmed reduction by hydrogen (H_2-TPR), temperature-programmed desorption (TPD) of O_2, $NO + O_2$, and C_3H_6, and temperature-programmed surface reduction (TPSR) of $NO + O_2$ under C_3H_6/He flow. The samples were also tested in a fixed-bed reactor for NO reduction with propene in the presence or absence of 1% O_2. This research was carried out to identify the different physicochemical properties of $LaFeO_3$ before and after Cu or Pd substitution, as well as to illustrate the correlation between the modification of their structure and their catalytic behaviors. Another objective of this work was to propose a reaction mechanism for NO reduction over Fe-based perovskites.

2. Experimental

A series of Fe-based mixed oxides was synthesized by reactive grinding in a manner similar to that reported previously [13–15]. Desired amounts of La_2O_3 (Alfa, 99.99%), Fe_2O_3 (Baker & Adamson, 97.49%), CuO (Aldrich, 99%), or PdO (Aldrich, 99.98%) were fully mixed and milled inside a tempered-steel vial using three tempered-steel balls under an air atmosphere. Grinding was conducted in two steps of 8 h for synthesis and 10 h for refining, with ZnO as the grinding additive.

The specific surface area of the samples calcined at 500 °C for 5 h was determined using an automated gas sorption system (NOVA 2000; Quantachrome) through nitrogen adsorption equilibrium at −196 °C. Before measurements were done, samples of about 200 mg were outgassed at 300 °C under vacuum for 6 h to remove any remaining humidity. The chemical composition (Fe, Cu, Pd) of the catalysts was established by atomic absorption spectroscopy (AAS) using a Perkin-Elmer 1100B spectrometer after the samples were dissolved in a mixture of 25 ml of 10% HCl and 2 ml of concentrated HF at 60 °C for 24 h. The amount of La in the perovskites was measured using an inductively coupled plasma (ICP) spectrometer (Optima 4300DV; Perkin-Elmer) with the same pretreatment before analysis as used for AAS. The final products were characterized by XRD using a Siemens D5000 diffractometer with Cu-K_α radiation ($\lambda = 1.5406$ Å) in a range $20° < 2\theta < 70°$ with steps of $0.05°(2\theta)$ each for 2.4 s. Crystallite sizes were determined using Scherrer's equation after considering the instrumental broadening, whereas the crystal phases were identified via the JCPDS reference. The morphology of the mixed oxides after calcination at 500 °C for 5 h was recorded at 100,000× magnification by scanning electron microscopy (SEM), using a JEOL JSM 840A at 110 kV.

H_2-TPR and TPD of O_2, $NO + O_2$, and C_3H_6 were conducted in a fixed-bed continuous-flow reactor. Before performing the H_2-TPR study, the sample (about 50 mg) was heated to 500 °C and maintained at this temperature for 1 h under 10% O_2. Before performing the TPD of O_2, $NO + O_2$, and C_3H_6-TPD, the sample was pretreated in 10% O_2, 3000 ppm $NO + 1\%$ O_2, and 3000 ppm C_3H_6, respectively, balanced by He, at 500 °C for 1 h, followed by cooling to room temperature under the same atmosphere and purging with He for 40 min. The sample was heated again from room temperature to 800 °C at a rate of 5 °C/min with a 20 ml/min 5% H_2/Ar flow in the TPR study, and the effluent gases were monitored on-line using a thermal conductivity detector (TCD). A cold trap was used to remove the water from effluent gas before it went through the TCD. The sample was flushed with 20 ml/min of He at a rising temperature up to 500 °C (800 °C for O_2-TPD) at a rate of 10 °C/min in the TPD analysis. The O_2, NO, N_2O, and N_2 desorbed during O_2-TPD and $NO + O_2$-TPD experiments were simultaneously detected and recorded on-line by mass spectrometry (MS) with mass numbers of 32, 30, 44, and 14, respectively. Moreover, C_3H_6, CO, and CO_2 desorbed during C_3H_6-TPD experiments were monitored with the mass numbers of 41, 28 and 44, respectively.

TPSR of $NO + O_2$ under C_3H_6/He flow over $LaFe_{0.8}Cu_{0.2}O_3$ was performed with the same sample pretreatment used for TPD of $NO + O_2$, but the thermodesorption was performed in 1000 ppm of C_3H_6/He instead of He. The desorbed C_3H_6, NO, and O_2 together with generated CO_2, N_2, and H_2O were monitored by MS with mass numbers of 41, 30, 32, 44, 14, and 18, respectively.

The selective catalytic reduction (SCR) of NO by C_3H_6 was conducted in a tubular fixed bed reactor at atmospheric pressure. A gas mixture of 3000 ppm of NO, 3000 ppm of C_3H_6, with or without 1% O_2, and the balance He, passed through

a catalyst bed charge of about 100 mg with a flow rate of 60 ml/min, yielding a space velocity of 50,000 h^{-1}. The reactor was placed in a tubular furnace controlled with a temperature programmer connected to a K-type thermocouple inserted inside the catalyst bed. The temperature was modified from 200 to 700 °C in 50 °C steps. The effluent gases (NO, N_2O, NO_2, and C_3H_6) were analyzed using a FTIR gas cell (FTLA 2000; ABB Inc.). N_2 and O_2 were monitored by gas chromatography (GC) (Hewlett Packard 5890) equipped with TCD and separated using columns of molecular sieve 13X combined with a silicone OV-101 column. Nitrogen oxides were also analyzed using a chemiluminescence $NO/NO_2/NO_x$ analyzer (model 200AH; Advanced Pollution Instrumentation). Organo nitrogen compounds, mentioned in the literature as intermediates of NO reduction by hydrocarbons [24–26], can be detected by comparing the NO_2 values from the NO_x analyzer and from the IR spectrometer. The higher NO_2 value from the NO_x analyzer was ascribed to the organo nitrogen compounds observed as an NO_2 signal after the NO_2/NO converter of this analyzer. These organo nitrogen compounds were further identified by GC-MS (CP 3800-Saturn 2200; Varian) and confirmed to be composed mainly of $C_3H_7NO_2$.

3. Results

3.1. Catalyst physicochemical characterization

The chemical compositions of the prepared solids established by AAS and ICP were close to the nominal values (Table 1). The BET specific surface areas and pore diameters of the materials, synthesized by reactive grinding after calcination at 500 °C for 5 h, were determined by N_2 adsorption and are also reported in Table 1. The results show a surface area about 30 m^2/g for the $LaFeO_3$ catalyst even after calcination at 500 °C. This value is superior to values from similar perovskites synthesized by ceramic methods [2,27]. The surface area of lanthanum ferrite is further enhanced upon Cu or Pd substitution, reaching a value >40 m^2/g.

A nearly pure orthorhombic $LaFeO_3$ perovskite-type structure (JCPDS card 74-2203) on all prepared Fe-based catalysts was confirmed by XRD patterns in Fig. 1, apart from a small amount of α-Fe_2O_3 (JCPDS card 86–0550). No diffraction lines corresponding to PdO (JCPDS card 85-0713) or CuO (JCPDS card 80-1917) are seen, suggesting that these metals are incorporated into the $LaFeO_3$ structure. However, the formation of tiny PdO or CuO particles, which could not be detected by XRD, cannot be excluded. The signal peak at $2\theta \approx 32°$ in XRD patterns implies a highly symmetric lattice

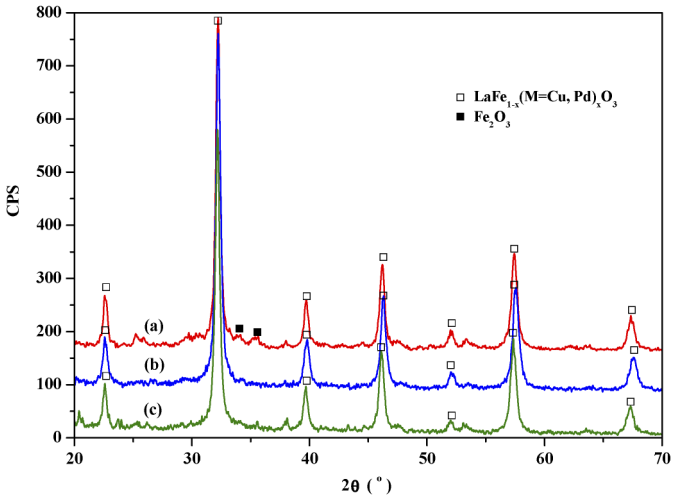

Fig. 1. XRD patterns of (a) $LaFeO_3$, (b) $LaFe_{0.8}Cu_{0.2}O_3$, (c) $LaFe_{0.97}Pd_{0.03}O_3$ mixed oxides.

inside the perovskites generated by reactive grinding [18]. Furthermore, the crystallite sizes were calculated using Scherrer's equation, as represented in Table 1 with values <20 nm. Taking into account the fact that both the pore diameters determined by N_2 adsorption and the crystallite sizes determined from XRD patterns are around 10–20 nm, we thus can infer that the porous structure of the present perovskites was formed via clustering of their primary particles, in accordance with earlier findings [28]. A sponge-like phase was observed by SEM (not shown) for all solids with a cluster of 50–200 nm, thought to be composed of individual nanoscale primary particles resulting in a somewhat porous microstructure. The dispersion of perovskite clusters seems to be improved by Cu or Pd substitution, yielding a higher specific surface area.

3.2. H_2-TPR

The reducibility of prepared samples was investigated by H_2-TPR experiments, as illustrated in Fig. 2. For $LaFeO_3$, three reduction peaks are detectable, suggesting a multiple-step reduction. The first small peak centered at 215 °C is followed by a second broad peak and a third more intense peak, overlapping substantially, with maxima at 440 and 573 °C, respectively. With 20% Cu substitution, the TPR profile of $LaFe_{0.8}Cu_{0.2}O_3$ exhibits two reduction signals, a sharp one centered at 241 °C and another centered at 460 °C with shoulders at 360 and 600 °C. As Fe is partially substituted by Pd, a more complicated reduction occurs, as shown in Fig. 2, with maxima at 78, 219, 328, and 465 °C, respectively.

Table 1
Properties of $LaFe_{1-x}M_xO_3$ (M = Cu or Pd) mixed oxides after calcination at 500 °C for 5 h

Sample	Chemical composition	Specific surface area (m^2/g)	Pore volume (ml/g)	Pore diameter (nm)	Crystallite size (nm)
$LaFeO_3$	$La_{0.99}Fe_{1.0}O_{3\pm\delta}$	30.5	0.13	16.2	18.7
$LaFe_{0.8}Cu_{0.2}O_3$	$La_{0.97}Fe_{0.80}Cu_{0.20}O_{3\pm\delta}$	41.6	0.16	14.6	16.8
$LaFe_{0.97}Pd_{0.03}O_3$	$La_{0.96}Fe_{0.97}Pd_{0.03}O_{3\pm\delta}$	48.1	0.15	11.8	18.9

Because La^{3+} is nonreducible under the conditions of H_2-TPR, the observed H_2 consumption should be ascribed to the reduction of Fe^{n+} ions in the case of $LaFeO_3$. A small amount of highly reducible Fe^{4+} has been reported in $LaFeO_3$ [29–31], and its reduction to Fe^{3+} occurred at $T < 300\,^{\circ}C$ during H_2-TPR experiments [30]. The small amount of H_2 consumed at 215 °C in the H_2-TPR profile of $LaFeO_3$ can be attributed to the reduction of Fe^{4+} to Fe^{3+}, followed by a successive reduction of Fe^{3+} centered at 440 and 573 °C, respectively. The quantitative analysis of these two peaks correlated well with the H_2 consumption in the reduction of Fe^{3+} to Fe^{2+}. They were therefore ascribed to $Fe^{3+} \rightarrow Fe^{2+}$ reduction occurring over the surface and in the bulk of $LaFeO_3$, respectively. Subsequently, the minor reduction peak above 700 °C was assigned to the partial reduction of Fe^{2+} to metallic iron. The formula of parent Fe-based perovskite was thus determined as $La_{0.99}Fe^{4+}_{0.055}Fe^{3+}_{0.945}O_{3.013}$ based on above ascription of Fe^{n+} reduction and elemental analysis (see Table 1), showing 5.5% Fe^{4+} and little overstoichiometric oxygen present in $LaFeO_3$. The additional peak at 241 °C appearing in the case of Cu-substituted perovskite can be attributed to the reduction of lattice Cu^{2+} to Cu^{+}, whereas the shoulder at 550 °C may be possibly ascribed to the complete reduction of Cu^{+} to Cu^{0}. These values are very similar to those observed in H_2-TPR of Cu/MCM-41 [21], $LaCo_{1-x}Cu_xO_3$, and $LaMn_{1-x}Cu_xO_3$ ($x = 0.1$, 0.2) [32,33]. The Fe^{4+} reduction peak is likely completely included in the rising part of the $Cu^{2+} \rightarrow Cu^{+}$ reduction peak, whereas the $Fe^{3+} \rightarrow Fe^{2+}$ reduction peak is shifted to lower temperatures in Cu-substituted samples, indicating that the Cu^{+} ions produced at this temperature interact with the iron ion, making the latter more easily reducible. A similar reduction behavior was found over $LaFe_{0.97}Pd_{0.03}O_3$ perovskite. An additional reduction peak was found in the $LaFe_{0.97}Pd_{0.03}O_3$ TPR trace at 78 °C, which, according to the literature [34], corresponds to the reduction of Pd^{2+} to Pd^{0}. This H_2 consumption occurring at quite low temperature reveals the excellent redox properties of Pd-substituted perovskite, possibly leading to good catalytic performance especially at low temperatures. $Fe^{4+} \rightarrow Fe^{3+}$ reduction was observed again at 219 °C along with a downward shift of $Fe^{3+} \rightarrow Fe^{2+}$ reduction in the H_2-TPR profile of $LaFe_{0.97}Pd_{0.03}O_3$ with respect to that of $LaFeO_3$.

3.3. O_2-TPD

TPD of O_2 over Fe-based perovskites was investigated; the results are shown in Fig. 3. The amount of O_2 released from perovskites was calculated after deconvolution of the O_2 desorption curve and are listed in Table 2. Only a small amount of O_2 desorbed from $LaFeO_3$ at $T < 700\,^{\circ}C$; this is designated as α-O_2 and ascribed to oxygen species weakly bound to the surface of the perovskite [14]. More O_2 desorption observed at $T > 700\,^{\circ}C$ is referred to as β-O_2, which is liberated from the lattice [14]. In the case of $LaFe_{0.97}Pd_{0.03}O_3$, a curve similar to that of $LaFeO_3$ was obtained apart from an obvious enhancement of β-O_2 desorption. Surprisingly, a broad and plateau-like α-O_2 desorption peak at 250–700 °C, along with a sharp β-O_2

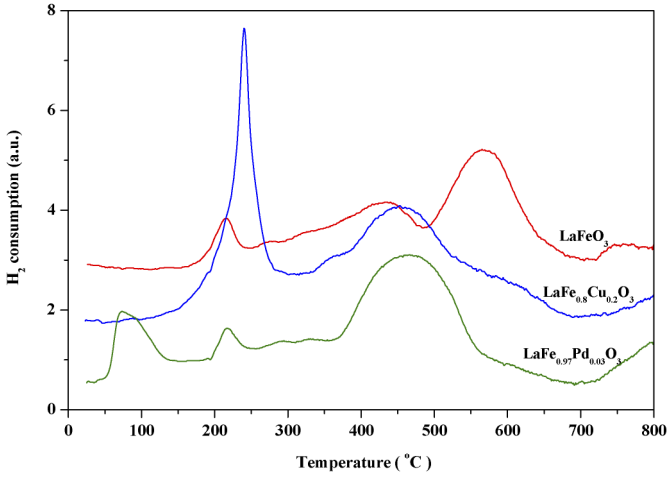

Fig. 2. H_2-TPR profiles of Fe-based perovskites.

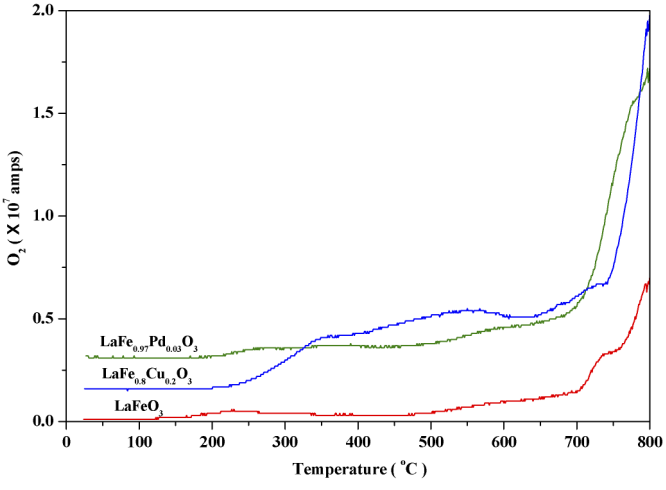

Fig. 3. TPD of O_2 profiles over Fe-based perovskites.

Table 2
Amount of O_2 desorbed from Fe-based perovskites during O_2-TPD experiments

Sample	Amount of oxygen desorbed[a]		Number of monolayers desorbed[b]	
	α-O_2 (μmol g^{-1}) <700 °C	β-O_2 (μmol g^{-1}) 700–800 °C	α-O_2	β-O_2
$LaFeO_3$	38.2	76.2	0.31	0.63
$LaFe_{0.8}Cu_{0.2}O_3$	196.5	202.2	1.18	1.22
$LaFe_{0.97}Pd_{0.03}O_3$	62.8	173.1	0.33	0.90

[a] Calculated by deconvolution of the O_2 desorption curves.
[b] Calculated with 4 μmol m^{-2} of oxygen per monolayer [14].

desorption maximum at 796 °C, were observed in the O_2-TPD profile over $LaFe_{0.8}Cu_{0.2}O_3$. This significant enhancement of adsorbed α-O_2 desorption is likely related to surface oxygen vacancies generated on Cu substitution.

3.4. $NO + O_2$-TPD

Figs. 4a–d show the desorption signals of NO ($m/e = 30$), N_2O ($m/e = 44$), N_2 ($m/e = 14$), and O_2 ($m/e = 32$) during the NO + O_2-TPD process after adsorption at room temperature under 3000 ppm NO and 1% O_2 for the three Fe-containing perovskites. Deconvolution of the NO + O_2-TPD profiles was performed using Lorentzian peak shapes in a computer peak-fitting routine. The amounts of NO, N_2O, N_2, and O_2 desorbed from perovskites were calculated based on these deconvolutions and are reported in Table 3. Three overlapping NO desorption peaks were observed for $LaFeO_3$ with maxima at 176, 272, and 360 °C, respectively. A similar NO desorption curve was observed over $LaFe_{0.97}Pd_{0.03}O_3$, except that its low-temperature peak was shifted upward and the third peak centered at 364 °C was slightly enhanced. A significant increase in the intensity of the third peak was found after Cu substitution. The N_2O and N_2 desorption (Figs. 4b and c) were detectable over the same range, 80–320 °C, followed by O_2 desorption at $T > 330$ °C over Fe-based perovskites (Fig. 4d).

3.5. C_3H_6-TPD

The MS signals of C_3H_6 ($m/e = 41$), CO ($m/e = 28$), and CO_2 ($m/e = 44$) during the TPD of C_3H_6 experiments over Fe-based perovskites are recorded in Figs. 5a–c. A quantitative analysis of the various gases desorbed from perovskites is presented in Table 4. One sharp peak for C_3H_6 desorption at 60 °C, and only minor CO or CO_2 desorption, are observed in the C_3H_6-TPD profile for $LaFeO_3$. C_3H_6 desorption is obviously decreased over the Cu-substituted perovskite, in combination with a significant CO_2 desorption with a maximum at 435 °C. This result implies that C_3H_6 transformation via complete oxidation into adsorbed CO_2 was promoted by Cu substitution. Taking into account the result that α-oxygen of Fe-based perovskites can be significantly enhanced by Cu substitution (see Fig. 3), it was thus thought that α-oxygen adsorbed on oxygen vacancies plays an important role in the transformation of C_3H_6 into CO_2. A similar diminution of C_3H_6 desorption was

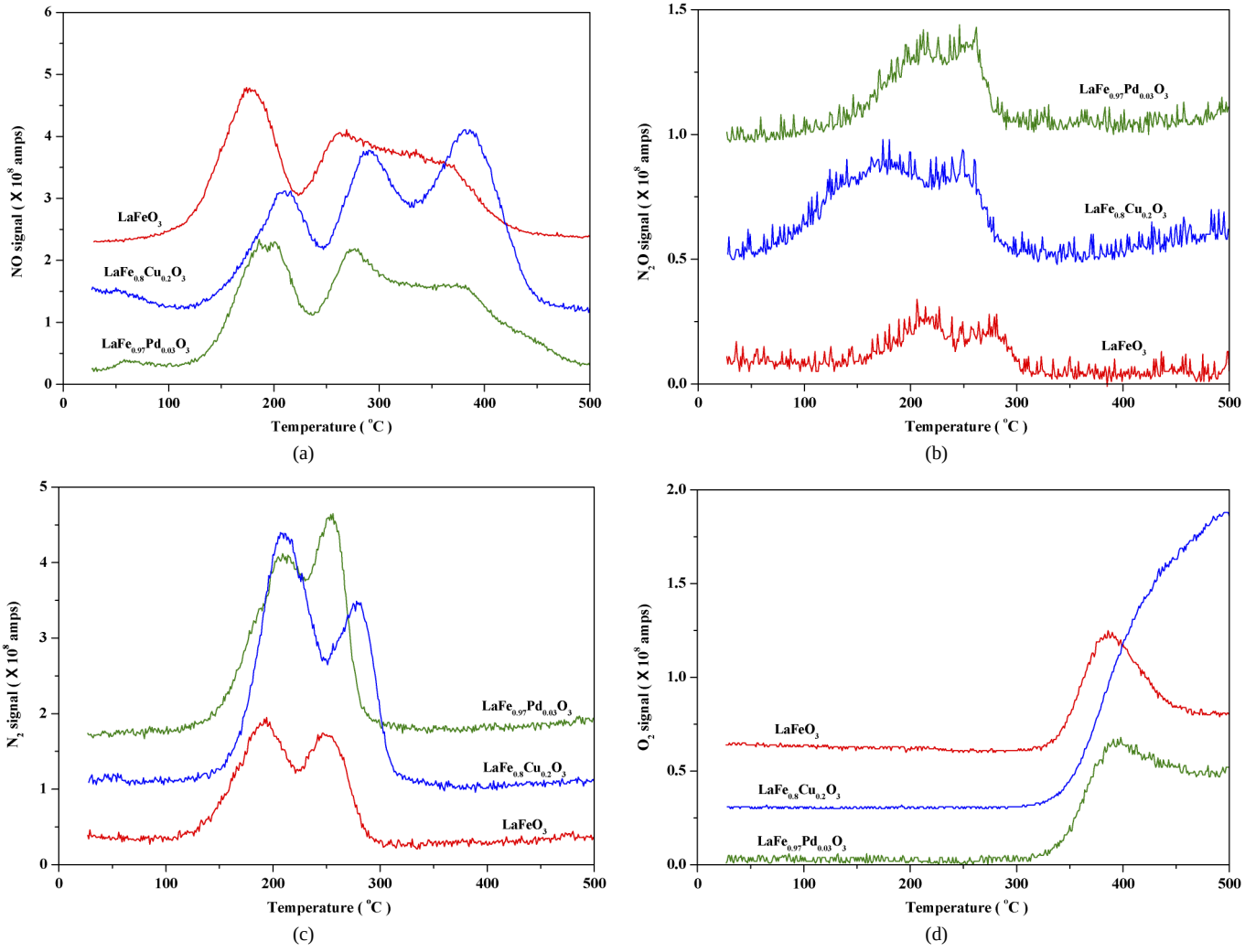

Fig. 4. TPD of NO + O_2 profiles over Fe-based perovskites. MS signal of (a) NO, (b) N_2O, (c) N_2, (d) O_2.

Table 3
Amounts of NO, N_2O, N_2 and O_2 desorbed from Fe-based perovskites during NO + O_2-TPD experiments

Sample	NO[a] (μmol g^{-1})				O_2 (μmol g^{-1})	Third NO/O_2[b]	N_2O (amp s)	N_2[c] (μmol g^{-1})		
	1	2	3	Total				1	2	Total
	176 °C	272 °C	360 °C					193 °C	250 °C	
$LaFeO_3$	19.1	19.5	10.6	49.2	11.3	0.94	2.1	2.0	1.1	3.1
	207 °C	293 °C	382 °C					211 °C	279 °C	
$LaFe_{0.8}Cu_{0.2}O_3$	15.3	20.3	27.9	63.5	28.2	0.99	4.5	3.9	1.8	5.7
	191 °C	279 °C	364 °C					209 °C	254 °C	
$LaFe_{0.97}Pd_{0.03}O_3$	15.5	19.8	16.3	51.6	15.5	1.05	2.8	2.8	1.8	4.6

[a] Calculated by deconvolution of NO desorption curves.
[b] The molar ratio between amount in the third NO desorption peak ($T > 300$ °C) and amount of O_2 desorbed over the same temperature range.
[c] Calculated by deconvolution of N_2 desorption curves.

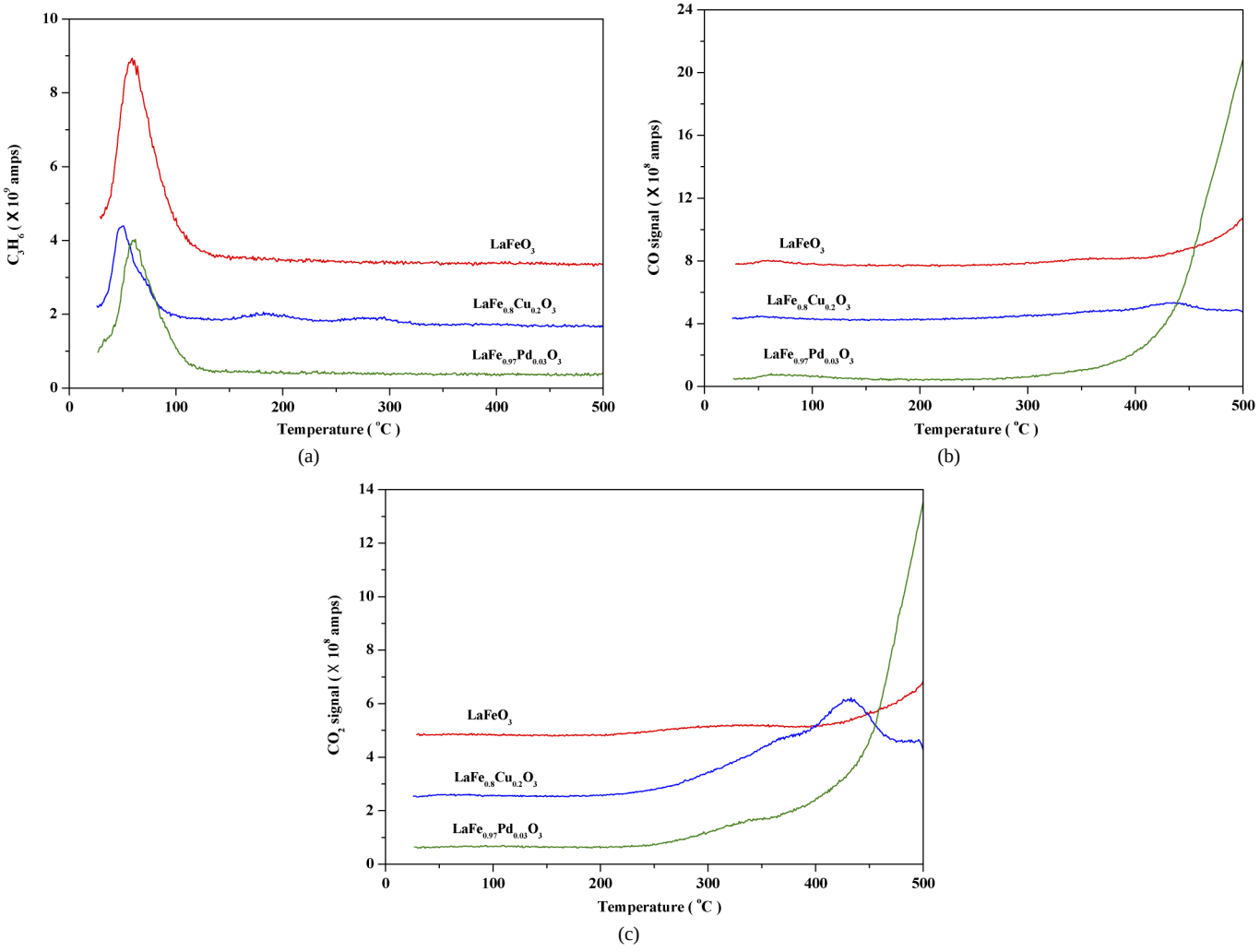

Fig. 5. TPD of C_3H_6 profiles over Fe-based perovskites. MS signal of (a) C_3H_6, (b) CO, (c) CO_2.

also found over $LaFe_{0.97}Pd_{0.03}O_3$. However, drastic increases in both CO and CO_2 desorption were achieved over this catalyst at $T > 200$ °C, suggesting that $LaFe_{0.97}Pd_{0.03}O_3$ is catalyzing not only the complete oxidation of C_3H_6 into CO_2, but also the partial oxidation of C_3H_6 into CO. This is likely related to the high reducibility of Pd^{2+} in lattice, as illustrated by the H_2-TPR profiles (Fig. 2).

3.6. TPSR of NO + O_2 under C_3H_6/He flow

The TPSR of adsorbed NO + O_2 in C_3H_6/He flow over $LaFe_{0.8}Cu_{0.2}O_3$ is presented in Fig. 6. A large amount of oxygen desorbs from the perovskite surface under an atmosphere of 1000 ppm C_3H_6/He. This signal rapidly declines at 240–280 °C simultaneously with the consumption of C_3H_6. At $T < 300$ °C,

Table 4
Amounts of C_3H_6, CO, and CO_2 desorbed from Fe-based perovskites during C_3H_6-TPD experiments

Sample	C_3H_6		CO		CO_2	
	T_{max} (°C)	Amount (μmol g^{-1})	T (°C)	Amount (μmol g^{-1})	T (°C)	Amount (μmol g^{-1})
$LaFeO_3$	60	3.5	>250	57.2	>200	72.9
$LaFe_{0.8}Cu_{0.2}O_3$	49	2.1	>250	34.0	>200	239.4
$LaFe_{0.97}Pd_{0.03}O_3$	60	2.3	>250	174.1	>200	342.7

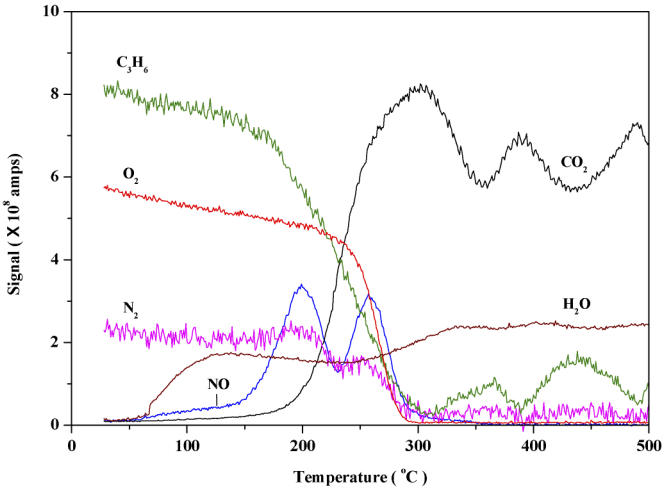

Fig. 6. MS signals during TPSR of NO + O_2 under C_3H_6/He flow over $LaFe_{0.8}Cu_{0.2}O_3$ perovskite. Conditions: flow rate = 20 ml/min, 3000 ppm NO, 1% O_2, 1000 ppm C_3H_6.

the NO desorption features are similar to those shown in Fig. 4a for the thermodesorption of NO; however, the third NO desorption peak at $T > 300$ °C seen in Fig. 4a is not present in Fig. 6. Some N_2 desorption is observed simultaneously with the NO desorption at $T < 300$ °C. The appearance of CO_2 coincides with the disappearance of C_3H_6.

3.7. Activity tests

The temperature dependence of NO conversion to N_2 over the three Fe-based perovskites is shown in Fig. 7a. Over unsubstituted $LaFeO_3$, the conversion to N_2 begins to be significant at 350 °C and increases progressively with increasing temperature, reaching 62% at 700 °C. A considerably enhanced conversion to N_2 was observed over lanthanum ferrite after Cu substitution, resulting in initiation at 350 °C and reaching values of 81% at 450 °C and 97% at 700 °C. A remarkable conversion to N_2, occurring at 250 °C and reaching as high as 67% at 350 °C, was achieved over $LaFe_{0.97}Pd_{0.03}O_3$. Organo nitrogen compounds were detected in the effluent at high temperature, with a maximum yield of 36% over $LaFeO_3$, 14% over $LaFe_{0.8}Cu_{0.2}O_3$, and 42% over $LaFe_{0.97}Pd_{0.03}O_3$, as depicted in Fig. 7b. These organo nitrogen compounds are widely mentioned in the literature as intermediates during SCR of NO by hydrocarbons [24–26]. The detection of these organo nitrogen compounds is simultaneous with a decrease in the conversion to N_2, as can be seen by comparing Figs. 7a and b. The conversion of C_3H_6, shown in Fig. 7c, increases progressively up to 80% at 200–500 °C. The conversion level at $T < 500$ °C was significantly improved after Cu and Pd substitution, resulting in C_3H_6 conversion of 63 and 68%, respectively, at 300 °C. Some CO formation was observed at high temperature, increasing in the following order: $LaFeO_3$ < $LaFe_{0.8}Cu_{0.2}O_3$ < $LaFe_{0.97}Pd_{0.03}O_3$ (Fig. 7d).

Fig. 8 presents the catalytic performance of $LaFe_{0.8}Cu_{0.2}O_3$ in NO reduction by C_3H_6 in absence of oxygen, showing a maximum N_2 yield (70%) at 350 °C followed by a decline (54%) at 450 °C and a final development (95%) at 700 °C. C_3H_6 conversion increased monotonically at rising temperature, reaching a plateau of approximately 45% at 500–600 °C and then rising continuously to almost 96% at 700 °C. Organo nitrogen compounds were found during this reaction, with a maximum of 30% at 450 °C over $LaFe_{0.8}Cu_{0.2}O_3$. Accompanied by the decreased yield of organo nitrogen compounds, CO formation became obvious at $T > 450$ °C and then reached about 30% at higher temperatures.

Yields of N_2 and organo nitrogen compounds and C_3H_6 conversions as functions of O_2 concentration over $LaFe_{0.8}Cu_{0.2}O_3$ at 400 °C are shown in Fig. 9 to clarify the role of gaseous O_2 during SCR of NO. With an increase in O_2 concentration, the maximum N_2 yield was about 76% at 3000 ppm O_2. Other authors have reported similar results for the effect of O_2 in SCR of NO by C_3H_6 for $La_{0.8}Sr_{0.2}Mn_{0.5}Cu_{0.5}O_3/Al_2O_3$ at 375 °C [35] and Cu/ZSM-5 at 300 °C [36]. The yield of organo nitrogen compounds decreases rapidly, from 23% in absence of O_2 to 1% at 5000 ppm O_2. In contrast, increasing O_2 concentration results in a monotonic increase in C_3H_6 conversion.

4. Discussion

4.1. O_2-TPD

The mobility of O_2 over Fe-based perovskites was investigated via O_2-TPD experiments; the results are given in Fig. 3 and Table 2. The lowest α- and β-O_2 desorption was obtained over $LaFeO_3$ among the three Fe-based perovskites, implying poor molecular O_2 coverage and lattice oxygen reducibility of lanthanum ferrite, in accordance with previous reports [37, 38]. The substitution of 20% Fe^{3+} by Cu^{2+} leads to a positive charge deficiency, which is compensated for by oxygen vacancies, resulting in significant enhancement of α-O_2. The β-oxygen of the Cu-substituted sample was also enhanced due to the improvement of its reducibility via Cu incorporation, as already confirmed by H_2-TPR experiments (Fig. 2). A similar effect was also found in the substitution of Fe^{3+} by Pd^{2+}. Note

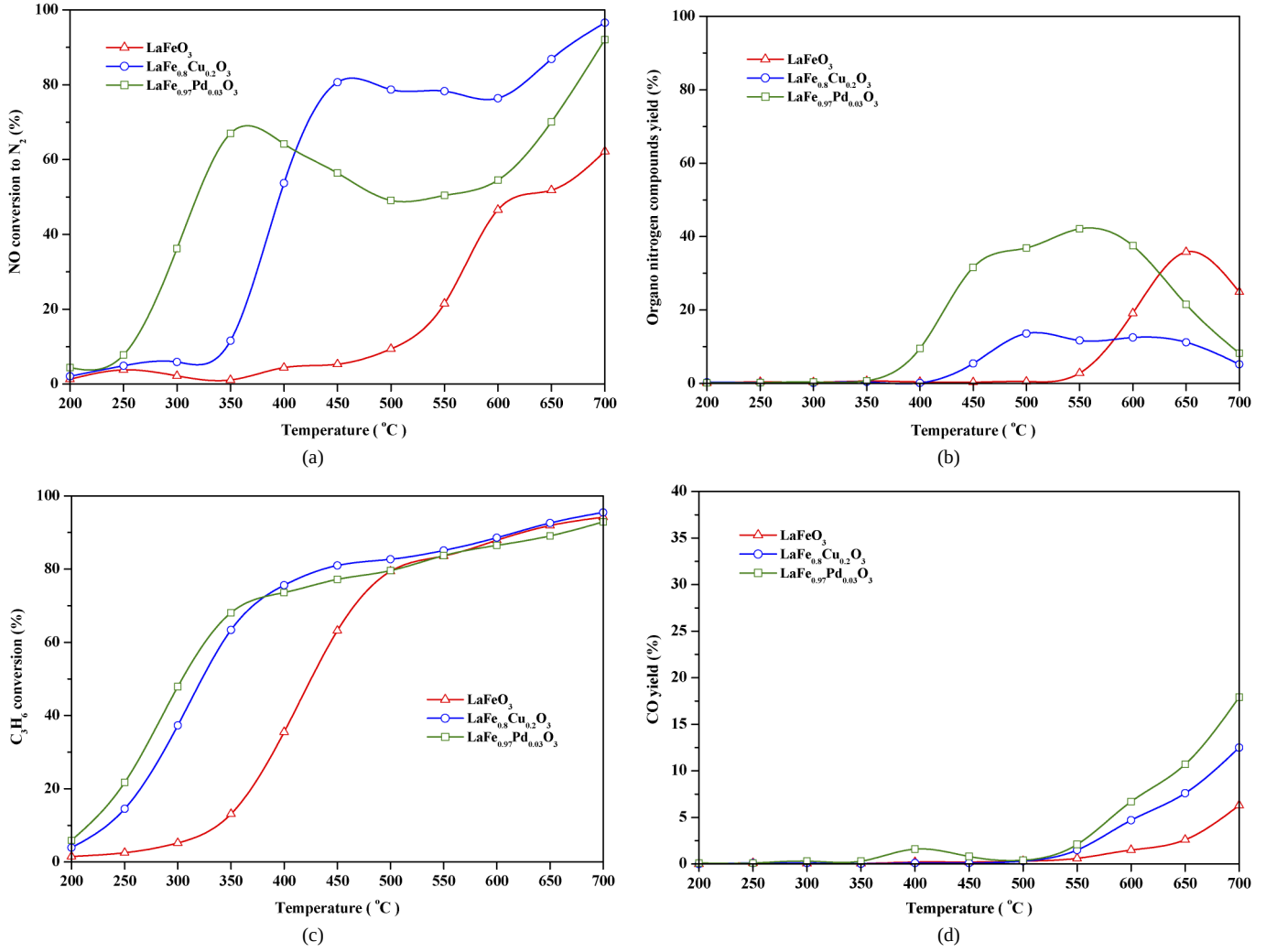

Fig. 7. (a) NO conversion to N_2, (b) yield of organo nitrogen compounds, (c) C_3H_6 conversion, (d) CO yield in $C_3H_6 + NO + O_2$ reactions over Fe-based perovskites. Conditions: GHSV = 50,000 h^{-1}, 3000 ppm C_3H_6, 3000 ppm NO, 1% O_2.

that β-O_2 can be significantly enhanced with only 3% substitution of B-site ions by Pd^{2+}. This likely corresponds to the highly reducible Pd^{2+} promoting the mobility of lattice O_2, as observed in H_2-TPR of $LaFe_{0.97}Pd_{0.03}O_3$ (Fig. 2). Based on our earlier description [14], the following process was assumed to occur during calcination of $LaFeO_3$ perovskite.

(1) Transient generation of anion vacancy during calcination of fresh sample,

$$\begin{matrix}\mathrm{OH} & & \mathrm{OH} & & & & \mathrm{O^-}\\ | & & | & & & & |\\ \mathrm{Fe}^{n+} & + & \mathrm{Fe}^{n+} & \xrightarrow{-\mathrm{H_2O}} & \underset{\text{(anion vacancy)}}{\mathrm{Fe}_{(n-1)+}\square} & + & \mathrm{Fe}^{n+},\end{matrix} \quad (1)$$

where $n = 3$ or 4.

(2) Instantaneous formation of α-O_2 by adsorbing O_2 at anion vacancy,

$$\mathrm{Fe}^{(n-1)+}\square + \mathrm{O_2} \rightarrow \begin{matrix}\mathrm{O_2^-}\\ |\\ \mathrm{Fe}^{n+}\end{matrix}. \quad (2)$$

The following two reactions are proposed for the α-O_2 desorption process:

$$\begin{matrix}\mathrm{O_2^-} & & \mathrm{O^-} & & & & \mathrm{O^{2-}}\\ | & & | & & & \swarrow & \quad \searrow\\ \mathrm{Fe}^{n+} & + & \mathrm{Fe}^{n+} & \rightarrow & \mathrm{Fe}^{n+} & & \mathrm{Fe}^{n+} & + \mathrm{O_2},\end{matrix} \quad (3)$$

$$\begin{matrix}\mathrm{O_2^-}\\ |\\ \mathrm{Fe}^{n+}\end{matrix} \rightarrow \mathrm{Fe}^{(n-1)+}\square + \mathrm{O_2}. \quad (4)$$

In Eqs. (1)–(4), iron ions are indicated here as examples. In the substituted samples, pairs of one Fe^{n+} and one Cu^{2+} or Pd^{2+} are also present. Reactions (1) and (3) may therefore happen on these new ion pairs. Reactions (3) and (4) also occur in the coordination sphere of copper or palladium ions.

The β-oxygen desorbed above 700 °C, as previously reported for similar compounds [38], is defined as the oxygen liberated from the lattice, leaving oxygen bulk vacancies and reduced cations. The amount of β-oxygen desorbed is thus generally considered a measure of lattice oxygen mobility. The $Fe^{n+} \rightarrow Fe^{(n-1)+}$ reduction ($n = 3$ or 4) and anion vacancy generation process after the desorption of lattice oxygen from

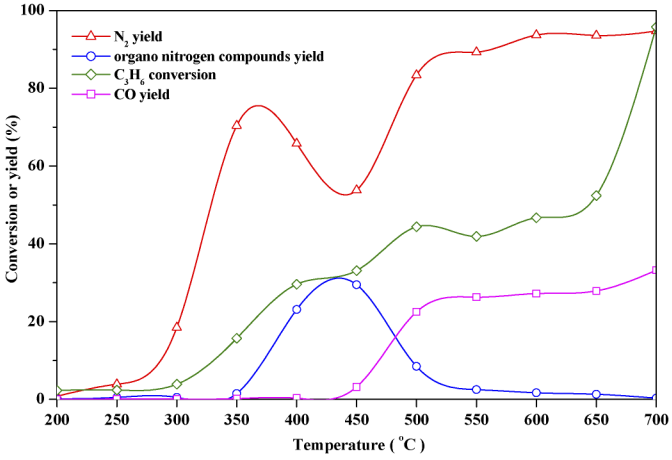

Fig. 8. Catalytic performance in $C_3H_6 + NO$ reaction over $LaFe_{0.8}Cu_{0.2}O_3$ perovskite. Conditions: GHSV = 50,000 h^{-1}, 3000 ppm C_3H_6, 3000 ppm NO.

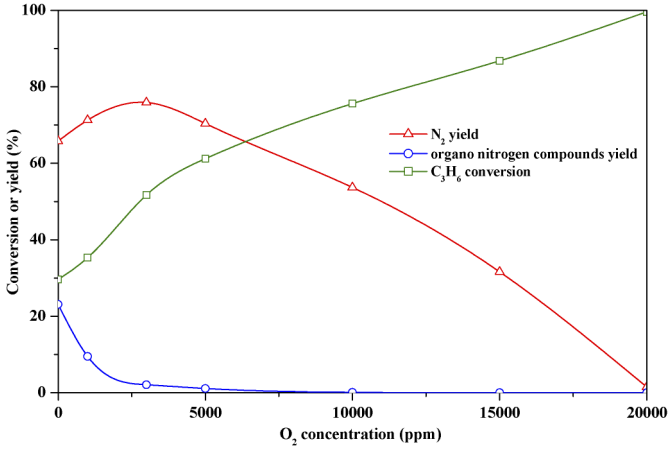

Fig. 9. Effect of O_2 feed concentration on NO reduction by C_3H_6 over $LaFe_{0.8}Cu_{0.2}O_3$. Conditions: GHSV = 50,000 h^{-1}, T = 400°C, 3000 ppm C_3H_6, 3000 ppm NO.

the surface, observed in H_2-TPR profiles (Fig. 2), was believed to involve the following step:

$$\underset{\text{(surface)}}{\overset{O^{2-}}{Fe^{n+}\quad Fe^{n+}}} \rightarrow \underset{\text{(surface)}}{Fe^{(n-1)+}\square Fe^{(n-1)+}} + \frac{1}{2}O_2. \tag{5}$$

Thereafter, β-oxygen desorption involves the diffusion of oxygen from the bulk to the surface,

$$\underset{\text{(surface)}}{Fe^{(n-1)+}\square Fe^{(n-1)+}} + \overset{O^{2-}}{\underset{\text{(bulk)}}{Fe^{n+}\quad Fe^{n+}}} \rightarrow \overset{O^{2-}}{\underset{\text{(surface)}}{Fe^{n+}\quad Fe^{n+}}} + \underset{\text{(bulk)}}{Fe^{(n-1)+}\square Fe^{(n-1)+}}. \tag{6}$$

In the case of Cu- and Pd-substituted samples, the desorption of β-oxygen can also be realized via the following step:

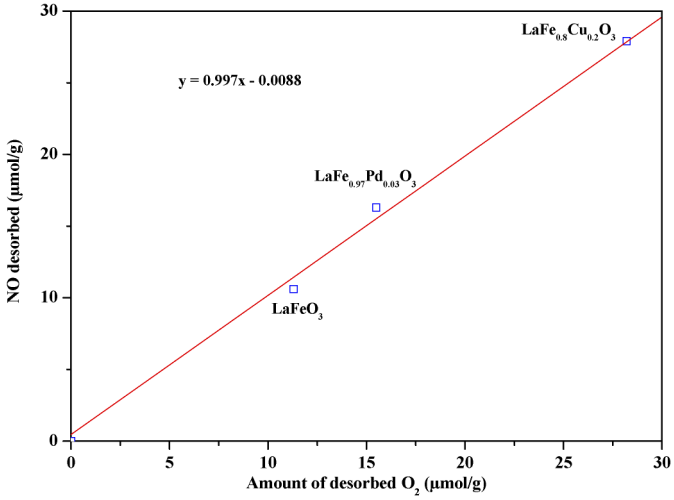

Fig. 10. Relationship between O_2 and the corresponding NO desorption at $T > 300\,°C$ during $NO + O_2$-TPD.

$$\underset{\text{(surface)}}{\overset{O^{2-}}{Fe^{n+}\quad M^{n+}}} \rightarrow \underset{\text{(surface)}}{Fe^{(n-1)+}\square M^{(n-1)+}} + \frac{1}{2}O_2,$$

M = Cu or Pd. (7)

In $LaFe_{0.8}Cu_{0.2}O_3$, the amount of β-oxygen desorbed at 700–800 °C was 202 μmol/g, which is half the theoretical oxygen corresponding to complete copper reduction to the metal (409 μmol/g). It seems thus that the β-oxygen thermodesorption corresponds to the reduction of Cu^{2+} to Cu^{+} as suggested by reaction (7).

4.2. $NO + O_2$-TPD

Various bands assigned to mononitrosyl, dinitrosyl, and nitrite or nitrate species were found in IR spectroscopy studies of NO adsorbed over $LaFeO_3$ perovskites [39]. The formation of nitrosyl, nitrite, or nitrate species during NO-TPD over Cu/MCM-41 was also observed in our previous work [21]. In the present work, the species adsorbed during co-adsorption of NO and O_2 over Fe-based perovskites were investigated by monitoring the MS signals of NO, N_2O, N_2, and O_2 in the effluents of $NO + O_2$ experiments (Figs. 4a–d). The amounts of the various species desorbed were quantified and listed in Table 3.

Although the NO desorption traces ($m/e = 30$) for Fe-based perovskites, reported in Fig. 4a, show essentially three overlapping peaks, the oxygen traces (Fig. 4d; $m/e = 32$) show that oxygen desorbs simultaneously with only the high-temperature NO peak in amounts that are essentially enhanced after Pd and Cu substitution (see Table 3). It is remarkable that the high-temperature NO peaks and O_2 peaks are essentially located at the same temperature and that even the shapes of the peaks look alike. Coq et al. [40] reported that the desorption of NO_3^- species would appear as a NO desorption peak at high temperature ($T > 300\,°C$) with parallel O_2 desorption. Furthermore, the moles of NO desorbed at the high-temperature peak are plotted against those of O_2 (Table 3) in Fig. 10. Given the imprecise nature of the curve fitting of NO traces, the data are reasonably

well fitted with a line of slope 1, indicating that the NO/O_2 ratio is essentially 1 over these catalysts. This strongly suggests that high-temperature NO desorption is associated with the desorption of an oxidized nitrogen oxide species with a general formula of NO_3^-. The oxidation of NO was likely realized by α-oxygen as O_2^- ion radicals formed during calcination and O_2 adsorption,

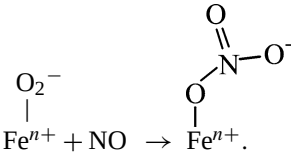

$$Fe^{n+} + NO \rightarrow Fe^{n+}. \quad (8)$$

Compared with Fig. 3, no α-oxygen desorbing at $T < 300\,^{\circ}C$ is observed in Fig. 4d, suggesting that reaction (8) involving α-oxygen occurs during the $NO + O_2$-TPD process.

The desorption of nitrate species leads to the formation of NO and O_2 with a molar ratio NO/O_2 equal to 1,

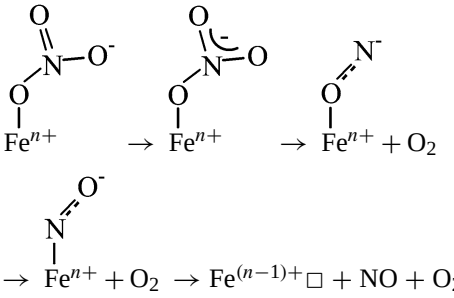

$$\rightarrow Fe^{n+} + O_2 \rightarrow Fe^{(n-1)+}\square + NO + O_2. \quad (9)$$

Besides the NO desorption related to nitrate species, the other two peaks in the NO traces of $NO + O_2$-TPD (Fig. 4a) show similar features among the three Fe-based perovskites, as does the desorption of N_2O and N_2 at 100–300 °C (Figs. 4b and c). The thermal stability of nitrogen-containing adspecies over Cu/ZSM-5 was enhanced with an increasing oxidation state of nitrogen [19]. In addition, both mononitrosyl and dinitrosyl species were weakly adsorbed on the same catalyst compared to nitrate species [41]. Therefore, the former two NO desorptions likely correspond to mononitrosyl and dinitrosyl species, respectively.

4.3. C_3H_6-TPD

C_3H_6 surface oxidation, which was enhanced by Cu substitution, was observed during C_3H_6 desorption over Fe-based perovskites, likely realized via suprafacial oxidation by α-O_2 bonded to anion vacancies. Based on our C_3H_6-TPD study, the following scheme may be proposed for the adsorption of C_3H_6 over perovskites. Using the site described by the left hand side of Eq. (3), the olefine should adsorb on the electron-deficient part of the site, as described in Eq. (10). The $-OC_3H_6\cdot$ radical (allylic adspecies) formed can now react with the surrounding α-O_2 to form CO_2 and water, as described previously [42],

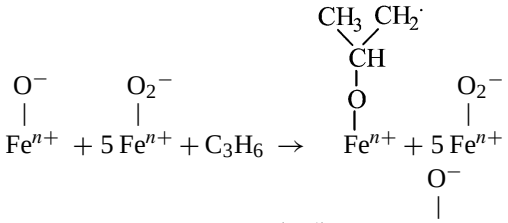

$$\rightarrow 3CO_2 + 3H_2O + 4Fe^{(n-1)+}\square + 2\,Fe^{n+}. \quad (10)$$

C_3H_6 adsorbed on the surface of the Pd-substituted sample can be transformed not only into CO_2 via complete oxidation, but also into CO via partial oxidation according to the C_3H_6-TPD experiments (Figs. 5a–c). The CO formation by hydrocarbon oxidation over Cu/ZSM-5 was reported to occur especially at low temperatures and to be higher from alkenes than from alkanes [43]. Although less abundant α-O_2 can be obtained over $LaFe_{0.97}Pd_{0.03}O_3$ than over $LaFe_{0.8}Cu_{0.2}O_3$ according to O_2-TPD experiments shown in Fig. 3, a higher content of adsorbed carbonaceous species was observed (see Table 4), indicating that the C_3H_6 transformation over Pd-substituted catalyst involves not only α-O_2, but also highly mobile lattice O^{2-}, due to the excellent redox properties of this catalyst, as illustrated in Fig. 2,

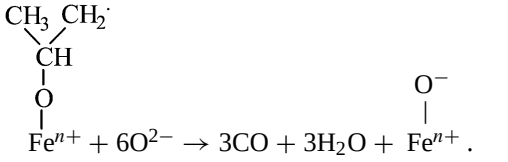

$$Fe^{n+} + 6O^{2-} \rightarrow 3CO + 3H_2O + Fe^{n+}. \quad (11)$$

4.4. TPSR of $NO + O_2$ under C_3H_6/He flow

Fig. 6 clearly shows that the NO desorption features observed at $T < 300\,^{\circ}C$ are similar to the two peaks assigned to mononitrosyl and dinitrosyl species in the TPD of $NO + O_2$ (Fig. 4a). Nevertheless, the NO desorption at high temperature ($T > 300\,^{\circ}C$) in Fig. 4a ascribed to nitrate species is no longer present in the traces of Fig. 6. This result implies that only the nitrate species among the adsorbed NO is highly active toward C_3H_6 and is completely consumed by this reducing agent. A significant NO conversion was indeed found in the activity tests at temperatures above 350 °C (Fig. 7a). At such high temperatures, only the nitrate species is present on the perovskite surface, another indication of the high reactivity of the nitrate species in the C_3H_6-SCR process.

As seen in Fig. 6, molecular oxygen desorbs even in the presence of C_3H_6 in the gas phase for temperatures below 260 °C, suggesting that the surface oxidation that consumes α-oxygen is not completed below this temperature. The CO_2 formed by this reaction desorbs from the surface essentially above 260 °C, indicating that either CO_2 or an oxygenated carbonaceous species leading to its formation is adsorbed on the perovskite surface above 260 °C.

N_2 was also detected during this experiment, again suggesting that reduction of the nitrate surface species by propene is associated with the SCR process.

4.5. Activity tests and reaction mechanism

Among the three Fe-based perovskite samples, the worst NO conversion to N_2 was achieved over unsubstituted $LaFeO_3$, with a significant NO reduction starting at 350 °C (where nitrate is the only remaining species over perovskites, according to the NO + O_2-TPD study) and a maximum of 62% at 700 °C (Fig. 7a). The high activity of nitrate species in reaction with propene was established via TPSR of NO + O_2 in C_3H_6/He tests, indicating that the formation of nitrate species is the first important step in NO reduction. This is in agreement with our previous findings in C_3H_6-SCR of NO over Cu-MCM-41 [21], $LaCo_{1-x}Cu_xO_3$ [32], and $LaMn_{1-x}Cu_xO_3$ [33]. Furthermore, organo nitrogen compounds, identified as composed mainly of 1-nitropropane (C_3H_7–NO_2) by GC-MS (typical composition: 92% $C_3H_7NO_2$, 4% C_2H_5–N=CO isocyanate, 2% $C_2H_5NO_2$, 1% CH_3O–NO, 0.5% C_3H_7O–NO, and 0.5% HCN), were detected at 550–700 °C during NO reduction over lanthanum ferrite (Fig. 7b), strongly implying a mechanism with organo nitrogen compounds as intermediates. The formation of organo nitrogen compounds via reaction of adsorbed hydrocarbons with the surface nitrate was reported as the rate-determining step in the SCR of the NO process [44–46]. The rate of nitrate consumption was also proven to be close to that of N_2 formation over Ce/ZSM-5 [46] and Al_2O_3 [47] according to FTIR kinetic studies. Hence the formation of 1-nitropropane should involve a reaction between the adsorbed species formed in reaction (10) and the nitrate species,

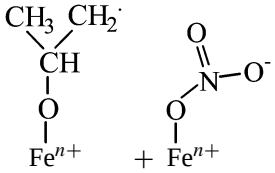

$$\xrightarrow{H_2O} CH_3\text{–}CH_2\text{–}CH_2\text{–}NO_2 + Fe^{n+}(O_2^-) + Fe^{n+}(OH). \quad (12)$$

A significantly improved N_2 yield was achieved after Cu incorporation into the B site of Fe-based perovskite. Besides the essential distinct effect of copper ions in the transformation of nitrogen oxides [19], Cu substitution promoted the formation of nitrate species due to the enhancement of α-oxygen, thereby further accelerating the generation of organo nitrogen compounds from nitrate and adsorbed propene, which is believed to be the rate-determining step in the SCR of NO by C_3H_6.

The reactivity of 1-nitropropane was investigated by Haj et al. [48]. This compound was found to be more rapidly decomposed in O_2 or NO + O_2 compared with C_3H_6, the final products being N_2, CO_2, and H_2O. This finding supports the fact that such species are highly reactive in the presence of O_2. Over Fe-based perovskites, the organo nitrogen compounds were detectable only in the gas phase at higher temperatures compared with N_2 formation. This seems to indicate a desorption rate of organo nitrogen compounds at 350–400 °C over $LaFe_{0.8}Cu_{0.2}O_3$ too low to allow detection. Based on a suggestion of Blower and Smith [49], further transformation of R–NO_2 into isocyanate (R–NCO) by a cyclic intermediate may be formulated as

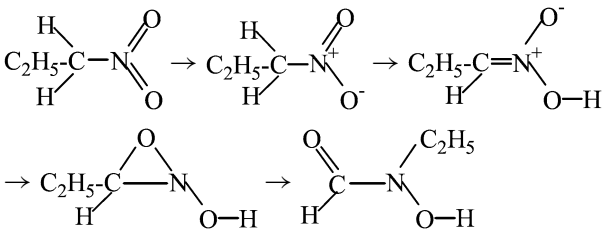

$$\xrightarrow{-H_2O} O{=}C{=}N\text{–}C_2H_5. \quad (13)$$

Finally, C_2H_5NCO was proposed to react with NO via the coupling of nitrogen atoms to yield the product of N_2 and CO_2 according to the assumption of Witzel et al [43]. At the same time, the participation of O_2 (especially α-oxygen) can promote the oxidation of the ethyl group into CO_2 and H_2O and accelerate the formation of N_2,

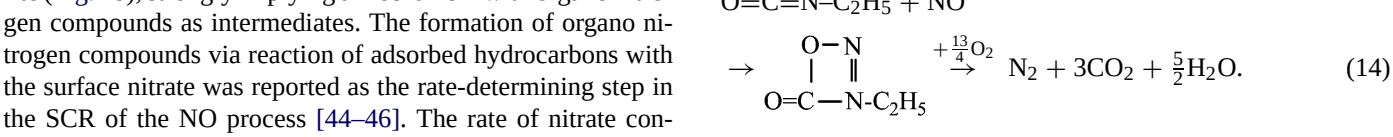

$$O{=}C{=}N\text{–}C_2H_5 + NO \xrightarrow{+\frac{13}{4}O_2} N_2 + 3CO_2 + \tfrac{5}{2}H_2O. \quad (14)$$

As the temperature rises above 450 °C, more organo nitrogen compounds are generated. These compounds accumulate over the surface of the Cu-substituted sample and even desorb into the gas phase, because they cannot transform into isocyanate fast enough, leading to a decline in N_2 formation due to the decreasing coverage of surface active sites.

Among the three Fe-based perovskites tested, the best catalytic performance at low temperature was observed over $LaFe_{0.97}Pd_{0.03}O_3$ (Figs. 7a–d), yielding the highest N_2 yield (approximately 67% at 350 °C) and the highest C_3H_6 conversion at $T < 400$ °C. The C_3H_6-TPD study revealed that the highest content of adsorbed carbonaceous species can be achieved over $LaFe_{0.97}Pd_{0.03}O_3$, followed not only by complete oxidation of C_3H_6 into CO_2 promoted by α-O_2, but also by partial oxidation of C_3H_6 into CO. This partial oxidation was related to the highly reducible lattice oxygen associated with Pd^{2+}, with the result that more CO was yielded over $LaFe_{0.97}Pd_{0.03}O_3$ during the SCR of NO (Fig. 7d). CO has been widely mentioned as an effective reducing agent to reduce NO at relatively low temperature with respect to C_3H_6 [1,3]. On the other hand, CO was reported to directly react with NO to form isocyanate (NCO) and final products [43,50]. This pathway avoids the formation of organo nitrogen compounds at relatively higher temperatures, resulting in outstanding activity at low temperatures. The abundant concentration of organo nitrogen compounds observed in the Pd-containing sample shown in Fig. 7b was ascribed to its higher ability in the formation of organo nitrogen compounds compared with $LaFeO_3$ and its lower ability to decompose organo nitrogen compounds compared with $LaFe_{0.8}Cu_{0.2}O_3$ due to a lower surface density of α-O_2. Generally, the outstanding catalytic characteristics of Pd-substituted perovskite for NO removal at low temperature were attributed mainly to its excellent redox properties (confirmed in the H_2-TPR study shown in Fig. 2), which can initiate the

redox reaction with a small energy barrier, leading to a partial oxidation of C_3H_6 into CO at low temperatures.

4.6. The role of O_2 in catalytic behavior of $LaFe_{0.8}Cu_{0.2}O_3$

Several points can be raised about the crucial role of O_2 based on the proposed mechanism. As a promoter, O_2 can oxidize NO into strongly adsorbed nitrate species and thus accelerate the formation of organo nitrogen compounds and isocyanate. As an inhibitor, O_2 can lead to the consumption of the reducing agent by the complete oxidation of C_3H_6. Ueda and Haruta reported that NO reduction with C_3H_6 barely occurs without oxygen over Au/Al_2O_3 [51], whereas in the present work we obtained a satisfying NO reduction by C_3H_6 in the absence of O_2 over $LaFe_{0.8}Cu_{0.2}O_3$ perovskite (see Fig. 8), achieving a higher N_2 yield at $T < 400\,^{\circ}C$ and a quite lower C_3H_6 conversion compared with those in the presence of 1% O_2. The maximum yield of 30% in organo nitrogen compounds shifted down to 450 °C, and more CO was formed under this reducing atmosphere. A detailed study of the effect of O_2 on catalytic performance of $LaFe_{0.8}Cu_{0.2}O_3$ at 400 °C is reported in Fig. 9, showing that NO conversion to N_2 passes through a maximum at 3000 ppm O_2, then tends to decline at higher O_2 concentrations. Taking into account the tendency toward increasing yields of N_2 and decreasing yields of organo nitrogen compounds at O_2 concentrations <3000 ppm, the observed increase in N_2 yield at low O_2 concentration can be ascribed to an acceleration of the decomposition of organo nitrogen compounds. In contrast, N_2 yields will be severely inhibited at O_2 concentrations >5000 ppm, because the unselective combustion of the reducing agent with O_2 becomes faster than the NO-SCR over Fe-based perovskites and diminishes the number of reductant molecules remaining for the SCR reaction. Indeed, Fig. 9 shows significant C_3H_6 consumption with increasing O_2 concentration.

5. Conclusion

In the current study, $LaFeO_3$ and the corresponding Cu- or Pd-substituted perovskites were synthesized by reactive grinding with nanoscale particle sizes <20 nm and high specific surface areas >30 m^2/g even after calcination at 500 °C for 5 h. Cu substitution of 20% Fe^{3+} in B sites leads to a positive charge deficiency that is compensated for by oxygen vacancies, resulting in significantly enhanced α-O_2 adsorption. The formation of nitrate species, which is highly reactive toward C_3H_6 according to TPSR tests, can be realized via oxidation of NO by α-O_2. Complete oxidation of C_3H_6 into CO_2 can also be promoted by this α-O_2.

Incorporation of Pd into B sites significantly improves the mobility of lattice O_2 and the reducibility of Fe-based perovskites. C_3H_6 transformation over Pd-substituted samples involves not only complete oxidation into CO_2 via α-O_2, but also partial oxidation into CO due to highly mobile lattice oxygen.

NO reduction by propene over Fe-based perovskites is controlled mainly by a mechanism involving organo nitrogen compounds, likely generated from the interaction between nitrate species and adsorbed C_3H_6. Subsequently, an isocyanate intermediate forms from organo nitrogen compounds and reacts with NO and/or O_2 to get the final products. With respect to $LaFeO_3$, the better performance achieved over Cu-substituted perovskite can be ascribed to the enhanced formation of nitrate species. High SCR activity over $LaFe_{0.97}Pd_{0.03}O_3$ is observed at $T < 350\,^{\circ}C$, suggesting a possible pathway involving the generation of isocyanate (NCO) by direct NO–CO interaction at low temperatures. This CO formation by propene oxidation readily occurs over Pd-substituted perovskites due to its outstanding redox properties.

A study of the effect of gaseous O_2 on the catalytic performance of $LaFe_{0.8}Cu_{0.2}O_3$ at 400 °C revealed that low O_2 concentrations can accelerate the decomposition of organo nitrogen compounds, resulting in improved NO reduction and C_3H_6 oxidation, whereas higher O_2 partial pressure reduces the yield of N_2 by depleting the reducing agent though complete C_3H_6 oxidation.

Acknowledgments

Financial support from the NSERC through its industrial chair program is gratefully acknowledged. The authors also thank Nanox Inc. for preparing the perovskite samples.

References

[1] A.E. Giannakas, A.K. Ladavos, P.J. Pomonis, Appl. Catal. B 49 (2004) 147.
[2] S.D. Peter, E. Garbowski, V. Perrichon, M. Primet, Catal. Lett. 70 (2000) 27.
[3] A.K. Ladavos, P.J. Pomonis, Appl. Catal. A 165 (1997) 73.
[4] J.C. Menezo, S. Inkari, T. Bertin, J. Barbier, N. Davias-Bainier, R. Noirot, T. Seguelong, Appl. Catal. B 15 (1998) L1.
[5] J. Lentmaier, S. Kemmler-Sack, Mater. Res. Bull. 33 (3) (1998) 461.
[6] M. Crespin, W.K. Hall, J. Catal. 69 (2) (1981) 359.
[7] A.E. Giannakas, T.C. Vaimakis, A.K. Ladavos, P.N. Trikalitis, P.J. Pomonis, J. Colloid. Interface Sci. 259 (2003) 244.
[8] R.J.H. Voorhoeve, D.W. Johnson Jr., J.P. Remeika, P.K. Gallagher, Science 195 (1977) 827.
[9] J. Kirchnerova, D. Klvana, Int. J. Hydrogen Energy 19 (1994) 501.
[10] X. Li, H.B. Zhang, X.X. Liu, S.J. Li, M.Y. Zhao, Mater. Chem. Phys. 38 (1994) 355.
[11] C. Xiulan, L. Yuan, J. Chem. Eng. 78 (2001) 205.
[12] G. Sinquin, C. Petit, J.P. Hindermann, A. Kiennemann, Catal. Today 70 (2001) 183.
[13] S. Kaliaguine, A. van Neste, US patent 6017504 (2000).
[14] S. Kaliaguine, A. van Neste, V. Szabo, J.E. Gallot, M. Bassir, R. Muzychuk, Appl. Catal. A 209 (2001) 345.
[15] V. Szabo, M. Bassir, A. van Neste, S. Kaliaguine, Appl. Catal. B 43 (2003) 81.
[16] M.L. Rojas, J.L.G. Fierro, L.G. Tejuca, A.T. Bell, J. Catal. 124 (1990) 41.
[17] L. Lisi, G. Bagnasco, P. Ciambelli, S. De Rossi, P. Porta, G. Russo, M. Turco, J. Solid State Chem. 146 (1999) 176.
[18] P. Porta, S. De Rossi, M. Faticanti, G. Minelli, I. Pettiti, L. Lisi, M. Turco, J. Solid State Chem. 146 (1999) 291.
[19] G. Centi, S. Perathoner, Appl. Catal. A 132 (1995) 179.
[20] M. Iwamoto, Catal. Today 29 (1996) 29.
[21] Y. Wan, J.X. Ma, Z. Wang, W. Zhou, S. Kaliaguine, J. Catal. 227 (2004) 242.
[22] N. Guilhaume, S.D. Peter, M. Primet, Appl. Catal. B 10 (1996) 325.
[23] Y. Nishihata, J. Mizuki, T. Akao, H. Tanaka, M. Uenishi, M. Kimura, T. Okamoto, N. Hamada, Nature 418 (2002) 164.

[24] K. Otsuka, R. Takahashi, I. Yamanaka, J. Catal. 185 (1) (1999) 182.
[25] A.D. Cowan, N.W. Cant, B.S. Haynes, P.F. Nelson, J. Catal. 176 (2) (1998) 329.
[26] T. Tanaka, T. Okuhara, M. Misono, Appl. Catal. B 4 (1994) L1.
[27] A.A. Leontiou, A.K. Ladavos, G.S. Armatas, P.N. Trikalitis, P.J. Pomonis, Appl. Catal. A 263 (2004) 227.
[28] S. Royer, A. van Neste, R. Davidson, S. McIntyre, S. Kaliaguine, Ind. Eng. Chem. Res. 43 (2004) 5670.
[29] S. Varma, B.N. Wani, N.M. Gupta, Appl. Catal. A 241 (2003) 341.
[30] P. Ciambelli, S. Cimino, L. Lisi, M. Faticanti, G. Minelli, I. Pettiti, P. Porta, Appl. Catal. B 33 (2001) 193.
[31] P. Porta, S. Cimino, S. de Rossi, M. Faticanti, G. Minelli, I. Pettiti, Mater. Chem. Phys. 71 (2001) 165.
[32] R.D. Zhang, A. Villanueva, H. Alamdari, S. Kaliaguine, Appl. Catal. B, in press.
[33] R.D. Zhang, A. Villanueva, H. Alamdari, S. Kaliaguine, Appl. Catal. A, in press.
[34] W.J. Shen, M. Okumura, Y. Matsumura, M. Haruta, Appl. Catal. A 213 (2001) 225.
[35] S. Wisniewski, J. Belkouch, L. Monceaux, Chem. 3 (2000) 443.
[36] M. Iwamoto, N. Mizuno, H. Yahiro, Stud. Surf. Sci. Catal. 75 (1992) 1285.
[37] L.G. Tejuca, J.L.G. Fierro, J.M.D. Tascón, Adv. Catal. 36 (1989) 237.
[38] T. Seiyama, N. Yamazoe, K. Eguchi, Ind. Eng. Chem., Prod. Res. Dev. 24 (1985) 19.
[39] L.A. Isupova, A.A. Budneva, E.A. Paukshtis, V.A. Sadykov, J. Mol. Catal. A 158 (2000) 275.
[40] B. Coq, D. Tachon, F. Figuéras, G. Mabilon, M. Prigent, Appl. Catal. B 6 (1995) 271.
[41] J. Valyon, W.K. Hall, J. Phys. Chem. 97 (1993) 1204.
[42] Y. Wan, J.X. Ma, W. Zhou, S. Kaliaguine, Appl. Catal. B 59 (2005) 235.
[43] F. Witzel, G.A. Sill, W.K. Hall, Stud. Surf. Sci. Catal. 84 (1994) 1531.
[44] R.H.H. Smits, Y. Iwasawa, Appl. Catal. B 6 (3) (1995) 201.
[45] M. Haneda, Y. Kintaichi, M. Inaba, H. Hamada, Catal. Today 42 (1998) 127.
[46] C. Yokoyama, M. Misono, J. Catal. 150 (1) (1994) 9.
[47] K.I. Shimizu, H. Kawabata, A. Satsuma, T. Hattori, J. Phys. Chem. B 103 (1999) 5240.
[48] K.O. Haj, S. Ziyade, M. Ziyad, F. Garin, Appl. Catal. B 37 (2002) 49.
[49] C.J. Blower, T.D. Smith, Zeolite 13 (1996) 394.
[50] J.W. London, A.T. Bell, J. Catal. 31 (1973) 96.
[51] A. Ueda, M. Haruta, Appl. Catal. B 18 (1–2) (1998) 115.